Redox Biology 53 (2022) 102340

Contents lists available at ScienceDirect

Redox Biology

journal homepage: www.elsevier.com/locate/redox

Electron transfer between cytochrome *c* and microsomal monooxygenase generates reactive oxygen species that accelerates apoptosis

Han Xie [a], Li Song [b], Sagie Katz [c], Jinyu Zhu [a], Yawen Liu [a], Jinping Tang [a], Linjun Cai [b], Peter Hildebrandt [c,**], Xiao Xia Han [a,*]

[a] State Key Laboratory of Supramolecular Structure and Materials, College of Chemistry, Jilin University, Changchun, 130012, PR China
[b] National Engineering Laboratory for AIDS Vaccine, School of Life Science, Jilin University, Changchun, 130012, PR China
[c] Department of Chemistry, Technische Universität Berlin, 10623, Berlin, Germany

ARTICLE INFO

Keywords:
Cytochrome *c*
ROS
Microsomal monooxygenase
Apoptosis
Resonance Raman spectroscopy

ABSTRACT

Generation of reactive oxygen species (ROS) are possibly induced by the crosstalk between mitochondria and endoplasmic reticula, which is physiologically important in apoptosis. Cytochrome *c* (Cyt *c*) is believed to play a crucial role in such signaling pathway by interrupting the coupling within microsomal monooxygenase (MMO). In this study, the correlation of ROS production with the electron transfer between Cyt *c* and the MMO system is investigated by resonance Raman (RR) spectroscopy. Binding of Cyt *c* to MMO is found to induce the production of ROS, which is quantitatively determined by the in-situ RR spectroscopy reflecting the interactions of Cyt *c* with generated ROS. The amount of ROS that is produced from isolated endoplasmic reticulum depends on the redox state of the Cyt *c*, indicating the important role of oxidized Cyt *c* in accelerating apoptosis. The role of electron transfer from MMO to Cyt *c* in the apoptotic mitochondria-endoplasmic reticulum pathway is accordingly proposed. This study is of significance for a deeper understanding of how Cyt *c* regulates apoptotic pathways through the endoplasmic reticulum, and thus may provide a rational basis for the design of antitumor drugs for cancer therapy.

1. Introduction

Controlled production of reactive oxygen species (ROS) is a physiologically important process in apoptotic pathways [1]. The membranous microsomal monooxygenase (MMO) system is thought to regulate generation of ROS through crosstalk between mitochondria and endoplasmic reticula (ER) [2]. The MMO on ER contains cytochrome P450 (CYP), its reductase (CPR) as well as a membrane bound cytochrome b_5 (Cyt b_5) unit with its NADH-dependent reductase [3]. The efficiency of electron transfer (ET) from NADPH via CPR to CYP for monooxygenation of substrates is known as the degree of coupling [4]. Cyt b_5 is considered to modulate CYP catalysis as it delivers the second electron needed for the CYP-catalyzed reactions, enhancing in the monooxygenase activity and coupling of such systems [5,6]. The MMO system is poorly coupled and believed to significantly contribute to the overall ROS production in the cell [7]. Production of ROS is an inevitable result of MMO uncoupling both in presence and in absence of substrates [7], leading to lipid peroxidation, cell toxicity, and death.

Cytochrome *c* (Cyt *c*) released from mitochondria is expected to form complexes with microsomal Cyt b_5 [8], which might interfere with the coupling between MMO constituents. CYP uncoupling subsequently results in a burst of MMO-dependent ROS generation, followed by amplified and strengthened pro-apoptotic signaling responses [2]. The association of Cyt *c* with Cyt b_5 is hypothesized to inhibit the CYP–Cyt b_5 interactions, but further detailed investigation of the function of the microsomal electron carriers is needed to check the hypothesis. Besides of Cyt b_5, the FMN domain of CPR in the MMO system is also an electron donor for Cyt *c*. ET to Cyt *c* takes place via transient interactions [9,10]. Since ET is crucial for the catalytic cycle of CYP [11], ROS production most likely involves ET between Cyt *c* and MMO. Exploration of ET between Cyt *c* and MMO will thus contribute to a better understanding of the mechanism of the Cyt *c*-mediated and MMO-dependent ROS generation.

Raman spectroscopy allows for probing structural information of

* Corresponding author.
** Corresponding author.
E-mail addresses: hildebrandt@chem.tu-berlin.de (P. Hildebrandt), hanxiaoxia@jlu.edu.cn (X.X. Han).

https://doi.org/10.1016/j.redox.2022.102340
Received 15 April 2022; Received in revised form 13 May 2022; Accepted 13 May 2022
Available online 18 May 2022

biomolecules under physiological conditions [12]. The intrinsically low sensitivity and selectivity of Raman signals can be remarkably improved *via* resonance Raman (RR) scattering where the excitation line is in resonance with an electronic transition of a chromophoric redox center of the target molecule. RR spectroscopy is particularly powerful for characterizing heme proteins and their processes, since the vibrational modes are sensitive markers for the redox state, the spin and ligation pattern of the heme iron [13–17]. Cyt *c*, Cyt b_5 and CYP are all heme proteins that exhibit high RR cross sections upon excitation in resonance with the Soret and Q-transition [18,19], facilitating investigation of ET between Cyt *c* and MMO. On the other hand, the vibrational modes of the heme are also sensitive to the reaction between Cyt *c* with ROS [20–22]. Thus, ROS generated due to the interactions of Cyt *c* with the MMO, can be indirectly determined by RR spectroscopy.

In this study, we investigated the ET between Cyt *c* and MMO (CYP3A4, containing CYP, its reductase, and Cyt b_5 in microsomes as shown in Scheme 1 to explore (1) if the presence of Cyt *c* influences ROS formation in the MMO system without substrates, (2) which redox state of Cyt *c* has a stronger impact on ROS formation, and (3) the possibility for MMO to transfer electrons to non-native states of Cyt *c*. By RR spectroscopy, ET between Cyt *c* and MMO are probed, and ROS produced by the association of Cyt *c* with MMO microsomes and with isolated ER from mouse liver are successfully quantified by RR spectra of Cyt *c*. For the first time, it is shown that ROS regulation by MMO is controlled by the redox state of Cyt *c*, and the underlying mechanism is proposed on the basis of RR spectroscopy and isothermal titration calorimetry (ITC). This study is a first attempt to investigate the Cyt *c*-mediated regulation of ROS production in the MMO system by RR spectroscopy, and it opens a new way to explore apoptotic mechanisms during the crosstalk between the mitochondria and ER.

2. Materials and methods

2.1. Materials

Horse heart Cyt *c* (C2867, ≥99% (SDS-PAGE)), CYP3A4 isozyme microsomes (C4982, with CPR and Cyt b_5, recombinant, expressed in baculovirus-infected insect cells), NADPH (β-Nicotinamide adenine dinucleotide 2-phosphate reduced, tetrasodium salt) (N7505), peroxide assay kit (MAK311), protease inhibitor cocktail (P8340), and endoplasmic reticulum isolation kit (ER0100) were all obtained from Sigma-Aldrich Co., Ltd. 6-week-old BALB/c female mice were bought from Liaoning Changsheng biotechnology co., Ltd. Ritonavir (R126586) was purchased from Shanghai Aladdin Biochemical Technology Co., Ltd. Acetonitrile, nickel chloride hexahydrate ($NiCl_2.6H_2O$, sodium hydroxide (NaOH), ethylene glycol, hydrazine hydrate (80%), hydrogen peroxide (H_2O_2, 30%) were purchased from Beijing chemical Co., Ltd. The PBS buffer (10 mM, NaCl, $Na_2HPO_412H_2O$, $NaH_2PO_42H_2O$, pH = 7.25) were prepared in ultrapure water (18.25 MΩ· cm).

2.2. Synthesis of Ni nanowires (Ni NWs)

The synthesis of Ni NWs followed dropping method [23]. Firstly, 2.4 g sodium hydroxide was dissolved in 70 mL ethylene glycol under continuous magnetic stirring for 1 h. Subsequently, 20 mL of hydrazine hydrate solution as a reducing agent was added with constant stirring to obtain a homogeneous solution. The as-prepared solution was then heated to 80 °C, followed by dropwise adding 10 mL of ethylene glycol of nickel chloride hexahydrate. After stirring for 10 min, the product of black fluffy solid was collected by an external magnet and washed with ethanol and distilled water for 3 times. The final product was dried at 60 °C in a vacuum oven for 12 h.

2.3. Preparation of reduced Cyt c

The as-prepared 10 mg Ni NWs was grinded and then mixed with 200 μL of oxidized Cyt *c* (400 μM) for 2 h at room temperature. The solution of reduced Cyt *c* was separated by collecting Ni NWs with a magnet.

2.4. Isothermal titration calorimetry (ITC)

Isothermal titration calorimetry (ITC) was carried out with an ITC equipment (Malvern Panalytical Ltd., MicroCal iTC200). All measurements were carried out under the conditions listed in Table S1 (Supplementary materials).

2.5. Samples in an anaerobic condition

The samples incubated in anaerobic condition were achieved in a glove box with nitrogen. All the reactions were completed in the glove box, and the solution were sealed rapidly in a hermetic cell before Raman measurements.

2.6. Instruments and measurements

The TEM images of CYP3A4 microsomes were obtained with a Jeol JEM 2100F microscope operating at 200 KV. RR spectra were obtained with a confocal microprobe Raman instrument (Renishaw Raman system model 1000), when using 532 nm excitation. The power at the sample was 10 mW. Each sample was measured for three cycles with 30 s acquisition time using a 50× Leica objective with a numerical aperture of 0.50 and a working distance of 8.2 mm. The samples were deposited in capillaries or aluminum plates before measurements.

For those RR spectra recorded with a 407 nm excitation, a confocal Raman spectrometer (LabRam HR-800, Jobin Yvon) with from a Kr^+ laser (Coherent Innova 300c) was used. The laser beam was focused by a 20× Nikon objective with a power of 1.0 mW at the sample (15s acquisition, 2 times accumulation). Here, all samples were mechanically rotated during the measurements to avoid laser-induced damage of the

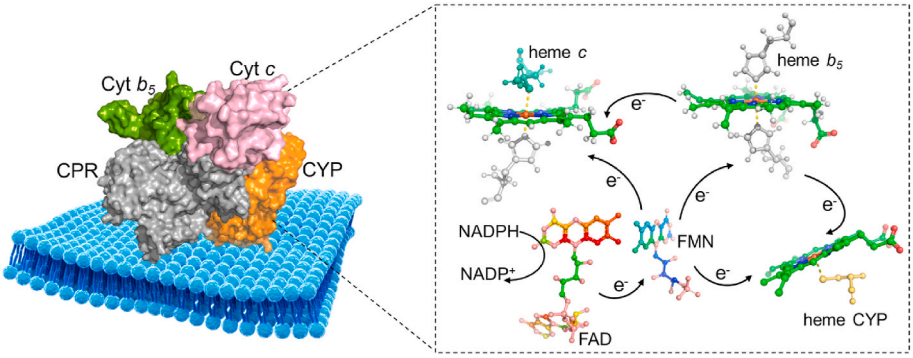

Scheme 1. A schematic presentation of the interaction of Cyt *c* with microsomal CYP3A4 and possible ET pathways in CYP3A4, and between Cyt *c* and CYP3A4.

proteins.

Details about the materials used in this study, preparation of smooth ER and peroxide assays are involved in supplementary materials. Smooth ER was obtained from the liver of 6-week-old BALB/c female mice, and the animal experiments were approved by the Institutional Animal Care and Use Committee of Jilin University.

3. Results

The CYP3A4 microsomes used in this study contained CYP, its reductase (CPR) and Cyt b_5, forming a complex (Scheme 1). Generally, the FMN domain of CPR either directly transfers electrons from NADPH and the FAD domain to CYP or indirectly to CYP via Cyt b_5 [24]. CYP can receive the first electron from the CPR and accept a second electron from either Cyt b_5 or CPR during the enzymatic reaction cycle of the CYP [25]. In the presence of oxidized cytochrome *c* (Cyt $c_{(ox)}$), ET might occur from Cyt b_5 to Cyt $c_{(ox)}$ [26], or from CPR to Cyt $c_{(ox)}$ as mentioned above. Possible ET pathways between Cyt *c* and the CYP3A4 microsomes are illustrated in Scheme 1.

3.1. ET from CYP3A4 microsomes to Cyt $c_{(ox)}$ and ROS generation

The microsomes used in this work were studied by transmission electron microscope (TEM) and the images are shown in Fig. 1A, in which lipid bilayers are clearly observed. Ni nanowires synthesized by a dropping method were used to reduce the Cyt $c_{(ox)}$ [23,27]. Using an excitation line of 532 nm in resonance with the Q-transition, the RR spectra displayed distinct RR fingerprints of Cyt $c_{(ox)}$ and Cyt $c_{(red)}$ (Fig. 1B, a and b). The assignment of the vibrational modes is well-established and briefly summarized in section 3 of the supplementary materials (Supplementary Fig. S1) [28]. Under anaerobic conditions, Cyt $c_{(ox)}$ was reduced and Cyt $c_{(red)}$ kept its reduced state in the presence of CYP3A4 microsomes and NADPH, as evidenced by Fig. 1B (c and d). These results suggested ET from CYP3A4 microsomes to Cyt $c_{(ox)}$. Under our experimental condition, Cyt $c_{(red)}$ was largely stable at room temperature in air for 30 min (Supplementary Fig. S2). In contrast, Cyt $c_{(red)}$ was oxidized upon mixing with NADPH-CYP3A4 (Fig. 1C). Notably, Cyt $c_{(ox)}$ was initially reduced and subsequently oxidized under the same conditions as in the experiments with Cyt $c_{(red)}$. Since oxidization of the Cyt $c_{(red)}$ by O_2 can be ruled out (Supplementary Fig. S2), Cyt $c_{(red)}$ was most likely oxidized by ROS [29], that were possibly generated during the ET processes among Cyt *c*, CYP3A4 and NADPH under aerobic conditions.

3.2. Quantification of H_2O_2

In the presence of NADPH and CYP3A4, Cyt $c_{(red)}$ and Cyt $c_{(ox)}$ initially remained in or are converted to the reduced form, respectively (labelled as "0 min" in Fig. 1C and D), followed by the oxidation as evidenced by the appearance of the oxidized band at 1635 cm^{-1}. These results point to the possibility of quantifying the generated ROS by the RR spectra of the Cyt *c*. Cyt $c_{(red)}$ can be oxidized by H_2O_2 [30]. Accordingly, H_2O_2 concentration-dependent RR spectra of Cyt $c_{(red)}$ were collected (Fig. 2A). The intensity ratio of the bands at 1635 and 1583 cm^{-1}, I_{1635}/I_{1583}, was used to monitor the extent of Cyt $c_{(red)}$ oxidation. A linear correlation was found for an intensity ratio from zero

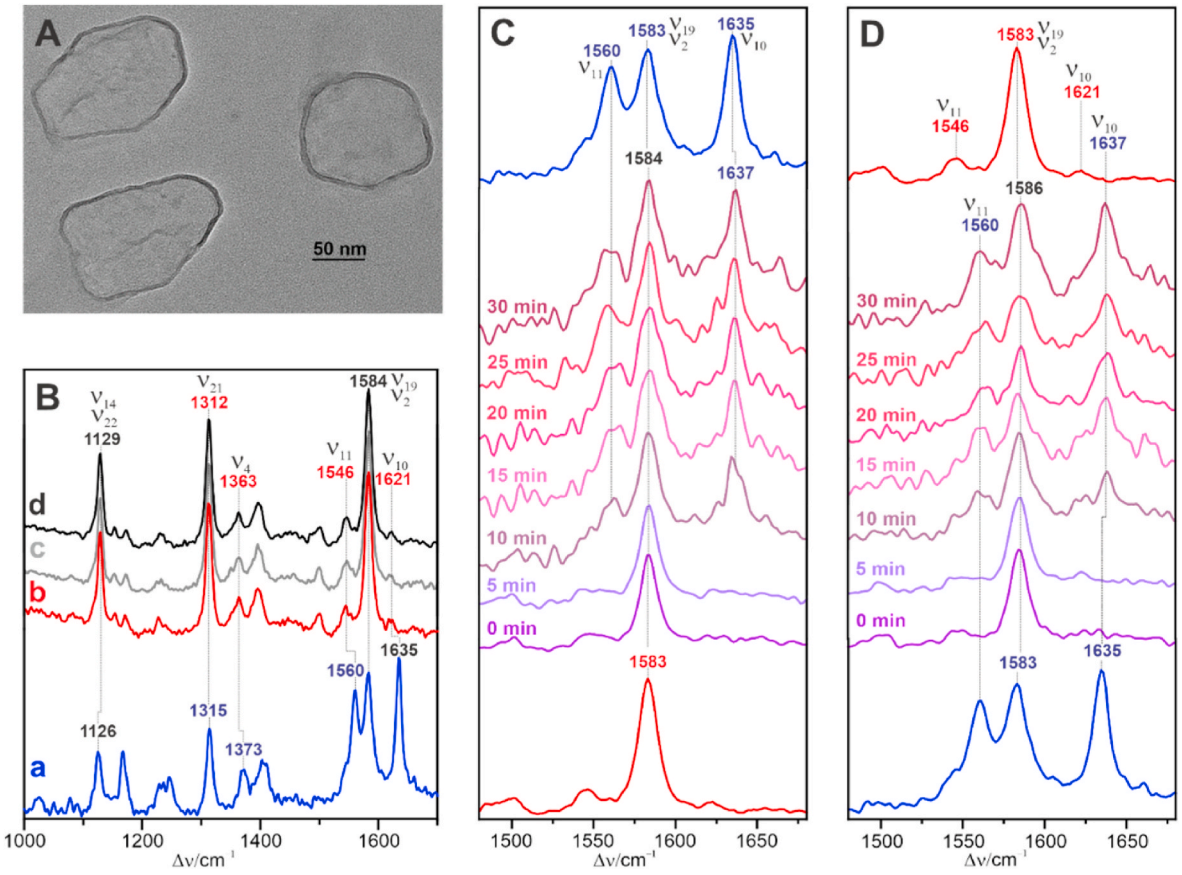

Fig. 1. (**A**) TEM image of the CYP3A4 microsomes; (**B**) RR spectra of (**a**) Cyt $c_{(ox)}$, (**b**) Cyt $c_{(red)}$, both in buffered solution at pH 7.4, and Cyt *c* with CYP3A4 and NADPH under anaerobic conditions (**c**: Cyt $c_{(ox)}$; **d**: Cyt $c_{(red)}$); time-dependent RR spectra of Cyt *c* with CYP3A4 and NADPH under aerobic conditions, starting from the bottom with Cyt $c_{(red)}$ (**C**) and Cyt $c_{(ox)}$ (**D**). The top spectra in **C** and **D** refer to oxidized and reduced form, respectively, and just serve for comparison. The concentrations of Cyt *c*, CYP3A4, and NADPH were 400 μM, 0.25 U, and 3.6 μM, respectively. The RR spectra were obtained with 532 nm excitation. (For interpretation of the references to colour in this figure legend, the reader is referred to the Web version of this article.)

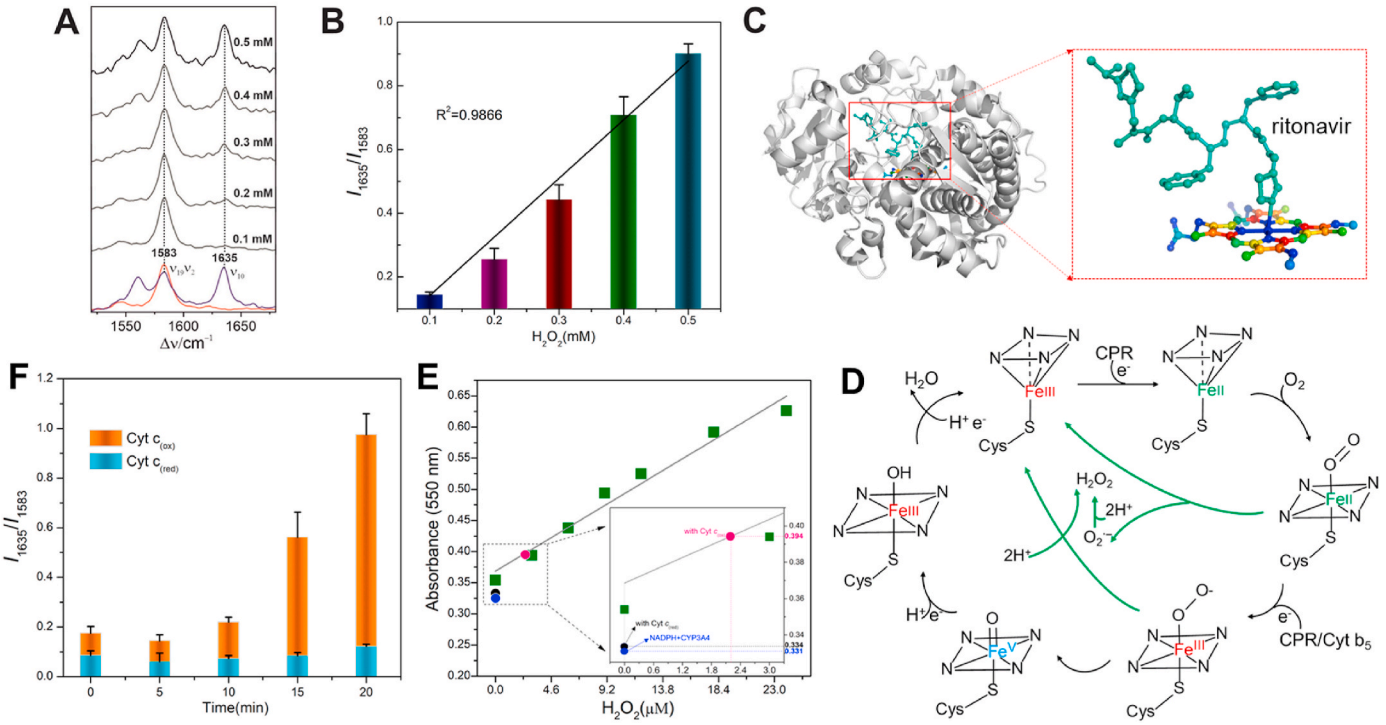

Fig. 2. (**A**), H_2O_2 concentration-dependent RR spectra of Cyt *c* measured with 532 nm excitation; the blue and red bottom spectra show the oxidized and reduced form of Cyt *c*, respectively; (**B**), calibration curve based on the H_2O_2 concentration and intensity ratio of the two bands at 1635 and 1583 cm^{-1}; (**C**) structure of CYP3A4 bound to ritonavir (PDB: 3nxu); (**D**) mechanism of ROS generation during the ET process; (**E**) calibration curve of the peroxide assay kit, including the results obtained from a mixture of (blue) NADPH and CYP3A4, (black) NADPH, CYP3A4 and Cyt $c_{(red)}$ and (pink) NADPH, CYP3A4 and Cyt $c_{(ox)}$. The inset shows a zoomed area of the plot in the range between 0 and 3.3 μM; (**F**) time-dependent changes of the intensity ratio I_{1635}/I_{1583} generated by NADPH and CYP3A4 from Cyt $c_{(red)}$ and Cyt $c_{(ox)}$. The concentrations used were 400 μM Cyt *c*, 0.03 U CYP3A4, and 1.2 μM NADPH. Each data point represents an average of five measurements, and each error bar indicates the standard deviation. (For interpretation of the references to colour in this figure legend, the reader is referred to the Web version of this article.)

up to ca. one, corresponding to an upper H_2O_2 concentration limit of ca. 0.5 mM (Fig. 2B). For higher H_2O_2 concentrations, the intensity ratio was not an appropriate spectral marker (Supplementary Fig. S3), most likely because both the ferric and the ferrous native as well as ferric non-native states include a RR band at ca. 1583 cm^{-1}, albeit with different relative RR cross sections. However, low ROS concentrations can be quantified based on this empirical correlation.

3.3. ROS generated from CYP and regulated by the redox state of Cyt c

The MMO on the ER is inefficient and poorly coupled, usually less than 50% [31]. The weak coupling may cause the ET chains of MMO to continue oxidizing NADPH and generating ROS even in the absence of any substrates (Fig. 2D) [4]. Without NADPH and H_2O_2 formation, Cyt *c* did not undergo denaturation compared with native Cyt $c_{(ox)}$. As shown in the Supplementary Fig. S4, the conformational change of ferric Cyt *c* in a mixture of Cyt $c_{(ox)}$ and CYP3A4 without NADPH (d) is negligible compared with the native Cyt $c_{(ox)}$ (brown), but the addition of NADPH significantly caused spectral changes (i.e., relative band intensities at 1560, 1583 and 1635 cm^{-1}) in trace c. Note that long incubation times of Cyt $c_{(red)}$ with CYP3A4 caused oxidation of Cyt *c* (b) with a similar spectral profile as the native Cyt $c_{(ox)}$. These results further provide that Cyt *c* can induce ROS formation. To further explore the origin of ROS, we added ritonavir to the mixture. Ritonavir perfectly fits into the CYP redox center and irreversibly binds to the heme iron [32]. The results (Supplementary Fig. S5) show that ritonavir inhibits the oxidation of Cyt $c_{(red)}$, evidently since no ROS were produced. Conversely, these findings further support the view that CYP is the origin of ROS in the absence of the inhibitor.

The H_2O_2 assay by a peroxide assay kit was conducted and the calibration curve was shown in Fig. 2E. In the presence of Cyt *c*, the concentration of H_2O_2 induced by Cyt $c_{(ox)}$ is around 2 μM (pink), but H_2O_2 was undetectable in the mixture of NADPH and CYP3A4 (blue), suggesting the addition of Cyt $c_{(ox)}$ leads to ROS formation. Additionally, ROS produced in the mixture of NADPH, CYP3A4 and Cyt $c_{(red)}$ is also undetectable (black), which is probably due to a smaller amount of H_2O_2 induced by Cyt $c_{(red)}$. However, the concentrations of H_2O_2 (induced by Cyt *c*) determined by this peroxide assay kit would be lower than their real concentrations because of the consumption of H_2O_2 by Cyt *c*. In the presence of Cyt *c* and catalytically small concentrations of CYP3A4, we observed an increase of oxidized Cyt *c* over the incubation time (Fig. 2F). Quantification on the basis of the calibration curve in Fig. 2B has shown that the amount of H_2O_2 induced by the Cyt $c_{(ox)}$ is more than 5 times larger than that induced by Cyt $c_{(red)}$ after 20 min incubation (Supplementary Table S2). These results suggest a redox-state specific role of Cyt *c* for ROS generation during the cross-talk between the mitochondria and ER.

3.4. ET to non-native Cyt c

Upon interactions with ROS (i.e. H_2O_2), oxidized Cyt *c* undergoes conformational changes. UV–Vis absorption spectra of Cyt $c_{(ox)}$ with H_2O_2 reveal a small red-shift of the Soret-band maximum (Supplementary Fig. S6). Qualitatively similar results were obtained upon addition of CYP3A4-NADPH to oxidized Cyt *c* (Supplementary Fig. S6). The underlying structural changes are also reflected by the RR spectra. A careful inspection of the RR spectra obtained after 30 min treatment of oxidized and reduced Cyt *c* with CYP3A4-NADPH (Fig. 1C and D) indicates an upshift of the heme modes ν_2/ν_{19} from 1583 to 1586 cm^{-1} and ν_{10} from 1635 to 1637 cm^{-1}. Since the RR spectra of CYP3A4 and NADPH are undetectable under our experimental condition with 532 nm excitation, the interference of the CYP with the RR spectrum of Cyt *c* is

ruled out (Supplementary Fig. S7). Thus, these band shifts point to a modification of the coordination sphere of the heme iron in Cyt *c* [33,34]. In fact, H_2O_2-induced covalent modifications of amino acid residues in Cyt *c* may cause the replacement of the Met80 axial ligand by another ligand [35]. We have further checked this hypothesis by analyzing the RR spectra of oxidized Cyt *c* at different time intervals following the addition of H_2O_2. For these experiments, we have employed Soret band excitation (407 nm; Supplementary, section 3, and Fig. S1) which specifically enhances the modes ν_4, ν_3, ν_2, and ν_{10} (Fig. 3B) [15,16,33]. The frequencies of these modes are sensitive spectral markers for the oxidation, spin, and ligation state of the heme [36]. The RR spectra display small frequency shifts of these modes that steadily increase with increasing incubation time (Fig. 3C). These spectral changes were analyzed on the basis of a global fit of the spectra with two components [37]. This approach assumes that the spectral changes result from the two-state conformational transition involving the native and a non-native oxidized state [38], denoted as B1 and B2, respectively (details of the analysis are given in the ssupplementary materials; section 4).

The marker modes also of B2 are at the position characteristic of a six-coordinate low-spin (6cLS) configuration as the native state B1. The slightly higher frequencies of these modes in B2, however, indicate the replacement of the Met80 ligand by a nitrogen-coordinating amino acid that could either be a His or a Lys [33,34,36,39,40]. In view of the recent mass-spectrometric analysis, the coordination by Lys appears to be most likely [41]. Assuming that the RR cross sections of the two 6cLS configurations are similar, one may determine the relative concentrations of both states as a function of the incubation time (Fig. 3D). This analysis is certainly a simplification since the non-native state B2 is known to release the new nitrogen-coordinating ligand and form a five-coordinate high-spin (5cHS) configuration, which exhibits only a relatively low RR cross section at Soret band excitation [38]. Hence, identification of its characteristic RR bands requires higher relative concentrations of the 5cHS species. However, the decrease of RR intensity with the incubation time (Fig. 3C) implies increasing heme degradation, for which a ferric 5cHS species may be a precursor [42].

In further experiments, we checked if non-native Cyt *c* can be reduced by electrons from CYP3A4 microsomes. It is unlikely for Cyt b_5

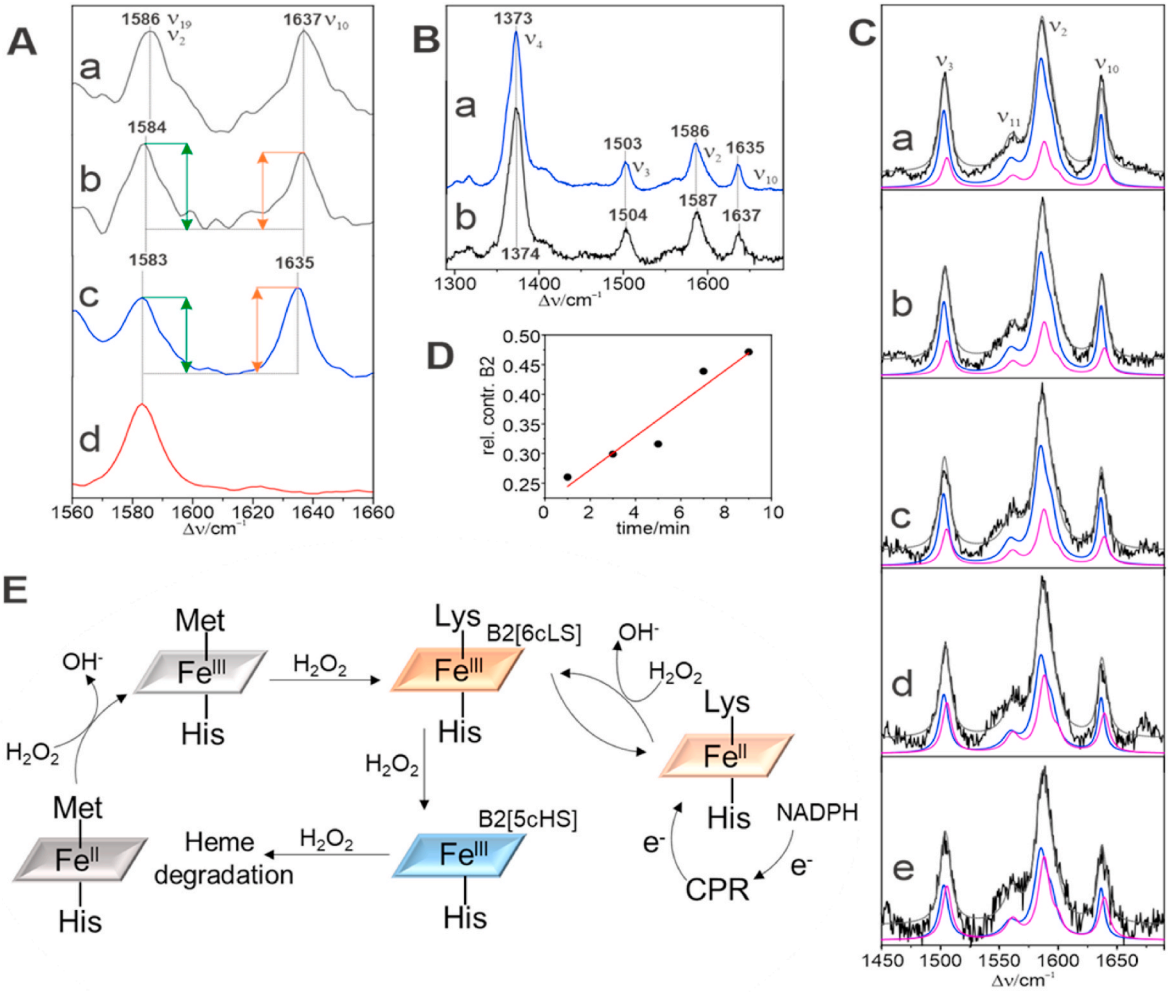

Fig. 3. (**A**), RR spectra of native Cyt *c* (B1) in buffered solution (pH 7.4) in the (**c**) oxidized and (**d**) reduced state, compared with the RR spectra of Cyt *c* obtained after 30 min-incubation of (**a**) ferric and (**b**) ferrous Cyt *c* with CYP3A4 and NADPH, taken from Fig. 1d and c, respectively. The spectra were obtained with 532 nm excitation. (**B**), RR spectra of (a) native oxidized Cyt *c* and the reaction product obtained after incubation with 5 mM H_2O_2 for 9 min, both measured with 407 nm excitation. (**C**) RR spectra of oxidized Cyt *c* incubated with 5 mM H_2O_2 for (**a**) 1 min, (**b**) 3 min, (**c**) 5 min, (**d**) 7 min, and (**e**) 9 min. The spectra were measured with 407 nm excitation. Solid and dotted black lines are the experimental traces and the fit of spectral components, respectively. The two component spectra that were employed are those of the native (B1) oxidized state (blue line) and a non-native (B2) 6cLS state (magenta line). Further details of the component analysis are given in the supplementary materials, section 4. (**D**) Relative concentrations of the non-native species B2 as a function of the incubation times as derived from the component analysis in Fig. 3C. (**E**) Possible reactions and ET among Cyt $c_{(red)}$, H_2O_2 and non-native Cyt *c*. (For interpretation of the references to colour in this figure legend, the reader is referred to the Web version of this article.)

to transfer electrons to non-native Cyt *c* that exhibits a negative redox potential, but it is possible for non-native Cyt *c* (6cLS, redox potential > -200 mV) [43] to accept electrons from CPR (FMN, redox potential = -270 mV) [44]. We first started the reaction of Cyt *c* (400 μM) by addition of CYP3A4 (0.25 U) and NADPH (3.6 μM) with 30 min incubation time that led to the formation of a considerable fraction of non-native B2(6cLS) (Fig. 1D). Subsequent addition of NADPH (3.6 μM) led to the immediate reduction of Cyt *c*, followed by re-oxidation due to the reaction with H_2O_2 (Fig. 4A). The process could be even repeated by additional application of NADPH. From our results (Fig. S8), NADPH can directly reduce non-native Cyt *c*, but in the presence of NADPH, Cyt b_5 would accept electrons from CPR [45]. Thus electron transfer from non-native Cyt *c* to Cyt b_5 is most likely impossible. Therefore, the re-oxidation of reduced non-native Cyt *c* originated from ROS formation. These results imply that despite the negative shift of the redox potential due to the ligand exchange [46], non-native Cyt *c* is likely reduced by electrons from CPR. This in turn is likely to affect MMO coupling and induces more ROS. Therefore, excessive NADPH will accelerate ROS generation in the presence of Cyt *c* at an early stage of apoptosis.

According to the above results, possible reactions and the ET among Cyt $c_{(red)}$, H_2O_2 and non-native Cyt *c* are displayed in Fig. 3E. H_2O_2 arising from the dismutation of $O_2^{\cdot-}$ is capable of oxidizing Cyt $c_{(red)}$, consistent with the result previously demonstrated [47]. Further reactions of Cyt $c_{(ox)}$ with H_2O_2 most likely causes replacement of Met80 by a Lys residue and form a non-native B2[6cLS] Cyt *c* [35]. Our results further revealed that the non-native Cyt *c* can accept electrons from CPR and change into a reduced Cyt *c*, which may be subsequently re-oxidized by the generated ROS. At the same time, the B2[6cLS] Cyt *c* may change into a B2[5cHS] configuration upon reaction with H_2O_2. Further reactions of the B2[5cHS] Cyt *c* finally cause degradation of the heme [35], as reflected by the decrease of the RR signals with increasing incubation of Cyt *c* with H_2O_2 (Fig. 3C).

3.5. Interactions of Cyt c with CYP3A4

To compare the binding affinity of the two Cyt *c* redox states to CYP3A4, we applied isothermal titration calorimetry (ITC). Fig. 4B and C shows the calorimetric titration and the integrated binding isotherm of the interactions of Cyt *c* with CYP3A4. The binding constants were determined to be $K_a = 1.09{\cdot}10^9\ M^{-1}$ (Cyt $c_{(ox)}$-CYP3A4) and $K_a = 5.70{\cdot}10^8\ M^{-1}$ (Cyt $c_{(red)}$-CYP3A4). The relatively higher binding affinity of Cyt $c_{(ox)}$ to CYP3A4 increases the probability of Cyt $c_{(ox)}$ to interfere with the more important role in the cross-talk between mitochondria and coupling of the MMO system through Cyt b_5 or CPR, inducing faster ROS production. Binding of Cyt *c* opens a reaction channel for ET from MMO to Cyt $c_{(ox)}$, at the expense of ET from Cyt b_5/CPR to CYP, thereby decreasing the enzyme coupling. These results are consistent with those shown in Fig. 2E. We thus conclude that the oxidized Cyt *c* plays a more important role in the cross-talk between mitochondria and endoplasmic reticula in the proapoptotic processes.

3.6. Cyt c-mediated ROS production from isolated smooth ER

Finally, we extended the RR experiments to smooth ER prepared from mouse liver cells (Fig. 5A). Details of the preparation are given in the supplementary materials, section 1. In mouse liver, the cytoplasmic side of smooth ER is known to contain CYP [48]. The morphology of smooth ER displayed continuous membranes, indicating successful isolation of the smooth ER (Fig. 5B).

Immediately after addition of oxidized Cyt *c*, rapid reduction took place as indicated by the lack of the characteristic ν_{10} mode in the RR spectrum at "0 min" (Fig. 5C). This marker band started to increase after ca. 20 min incubation and reached a value at 60 min that corresponded to an extent of ca. 30% oxidized Cyt *c*. These finding imply that similar as in the experiments with the recombinant proteins (Fig. 1D), also in ER rapid reduction of Cyt $c_{(ox)}$ takes place due to the reaction with NADPH/CYP, followed by a slower re-oxidation by ROS generated during the ET processes between Cyt *c*, CYP, and NADPH under aerobic conditions.

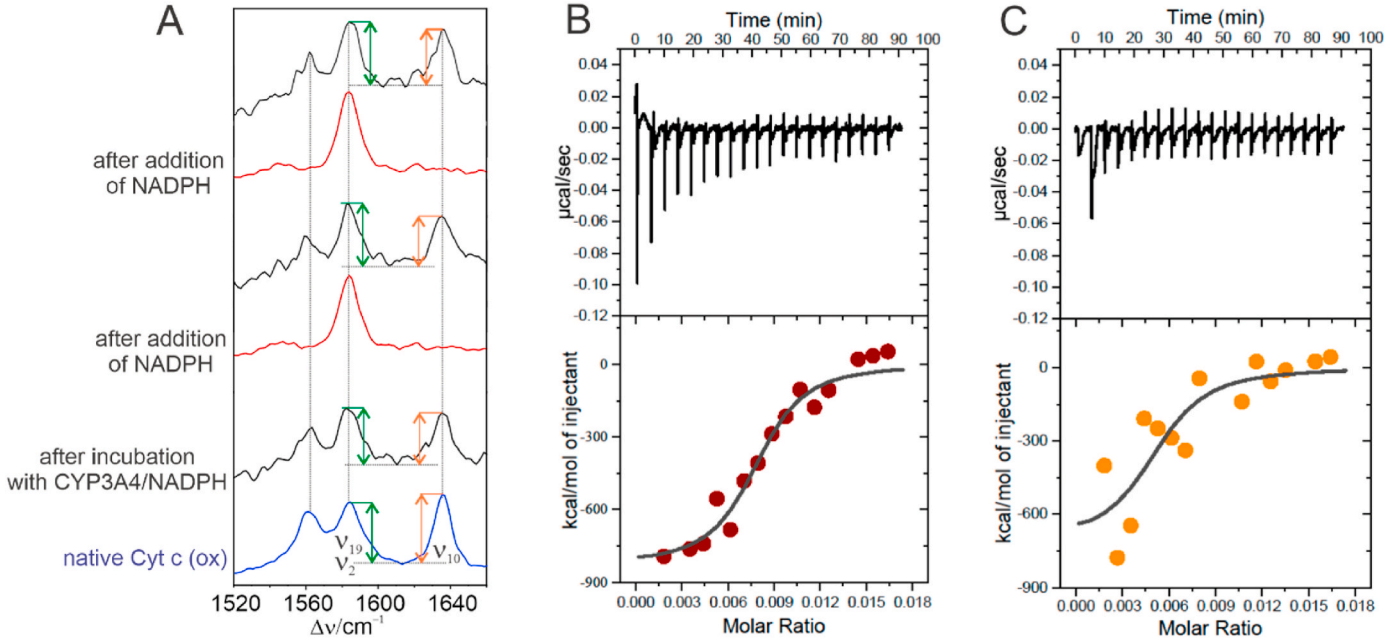

Fig. 4. RR spectra of Cyt *c* (400 μM) obtained with 532 nm excitation (**A**). The bottom (blue) spectrum represents the ferric native (B1) form of Cyt *c* with an intensity ratio I_{1635}/I_{1583} larger than 1. Upon reaction with ROS generated by CYP3A4/NADPH a fraction of Cyt *c* is converted to the non-native form as reflected by lower intensity ratio (<1) of these bands. Addition of NADPH (3.6 μM) reduces both the native and non-native Cyt *c* and the reaction H_2O_2 is restarted. This reaction sequence was repeated again, confirming the reduction of non-native Cyt *c* by CYP3A4/NADPH. (**B**) and (**C**) show the calorimetric titration and the integrated binding isotherm of the interaction of CYP3A4 with Cyt $c_{(ox)}$ Cyt $c_{(red)}$, respectively. (For interpretation of the references to colour in this figure legend, the reader is referred to the Web version of this article.)

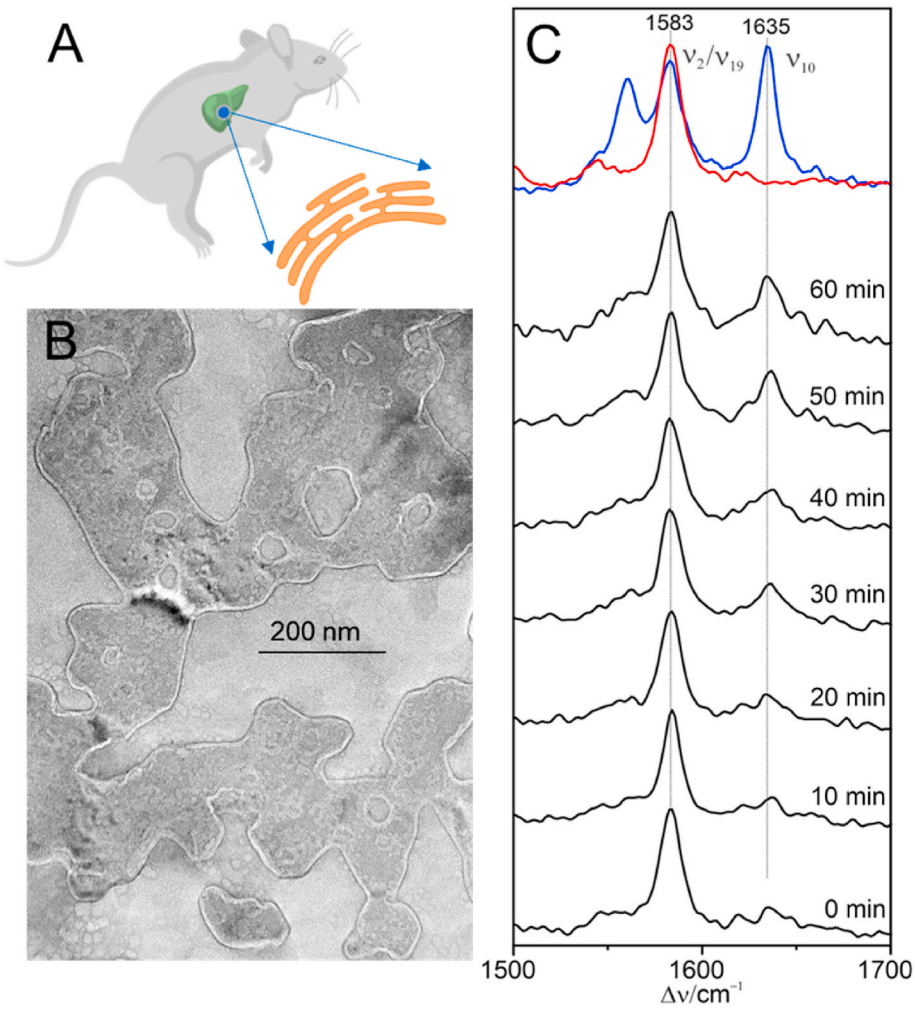

Fig. 5. ROS production from isolated smooth ER of mouse liver due to interaction with Cyt *c*. **(A)** Schematic illustration of ER isolation; **(B)** TEM image of isolated smooth ER; **(C)** RR spectra of smooth ER with Cyt $c_{(ox)}$ (400 μM) in the presence of NADPH (10 μM) under aerobic conditions after different incubation times. The red and blue traces refer to the pure reduced and oxidized Cyt *c* spectra as a reference. RR spectra were measured with 532 nm excitation. (For interpretation of the references to colour in this figure legend, the reader is referred to the Web version of this article.)

The only difference compared to the experiments in Fig. 1D is the slower re-oxidation rate, presumably due to the restricted mobility and lower concentration of CYP. This is most likely the reason why upon addition of reduced Cyt *c* to smooth ER no re-oxidation is observed within 60 min incubation (Supplementary Fig. S9). These data confirmed the above conclusion that the oxidized Cyt *c* plays a crucial role in ROS generation,

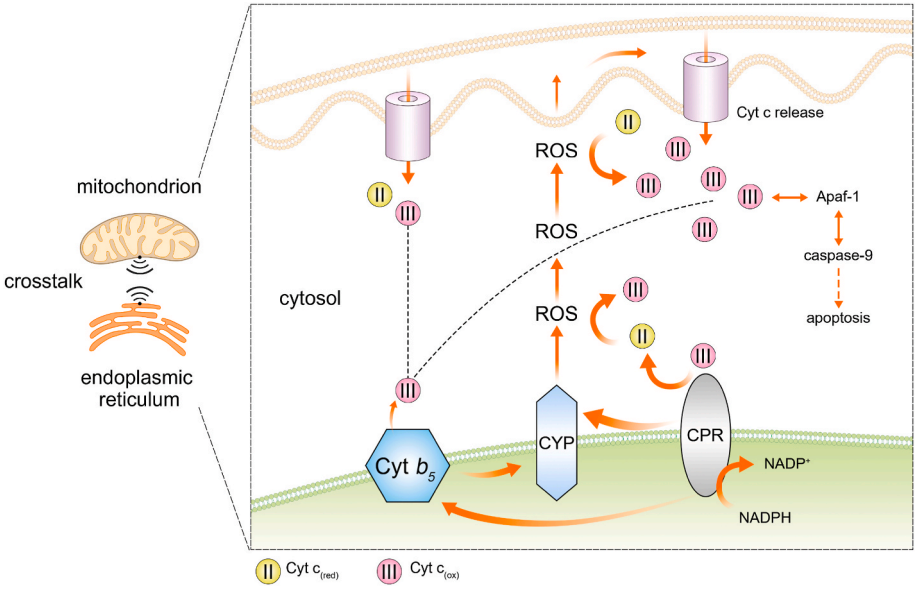

Fig. 6. A proposed mechanism about the role of Cyt $c_{(ox)}$ in regulating ROS generation and accelerating apoptosis during crosstalk between mitochondria and ER.

which will accelerate apoptosis through the mitochondria-ER pathway.

4. Discussion

At an early stage of apoptosis when there are yet only limited amounts of Cyt *c* released from mitochondria, the impact of Cyt *c* on ROS generation depends on its redox state. The reduced Cyt *c* has a lower binding affinity to the MMO system on the ER, and it can induce ROS generation, but only less efficiently. When oxidized Cyt *c* binds to the MMO system through Cyt b_5 or CPR, it will promptly induce ROS production owing to higher binding affinity and ET communication with the MMO. Additionally, the produced ROS also oxidize Cyt $c_{(red)}$, promoting binding of Cyt *c* to the MMO system, and thus a further increase of ROS production. The accumulated ROS subsequently cause the release of more Cyt *c* from the mitochondria, which further accelerates the Cyt *c* binding and ROS production (Fig. 6). Our study also suggested that ROS production is highly dependent on the electron donors (e.g., NADPH).

It was proven that the redox state of Cyt *c* regulates cell fate through the Apaf-1/caspase 9 pathway. In a living cell, the cytosol is a reducer environment and most Cyt *c* keeps its reduced form, but in an apoptotic cell, the reducer environment is disturbed and the increasing oxidized Cyt *c* accelerates apoptosis [49,50] The present results reveal an alternative pathway based on Cyt *c*-ER cross-talk that accelerates apoptosis by ROS generation through the interactions of Cyt *c* with MMO system. Importantly, both pathways underline the important proapoptotic role of oxidized Cyt *c*. Our results provide further insight into the role of ET between Cyt *c* and the MMO system for ROS generation outside the ERs, and thus for the redox-dependent regulation of apoptosis by Cyt *c*.

5. Conclusions

In this study, we investigated the interaction of Cyt *c* with the microsomal MMO system by RR spectroscopy. The correlation of the ET from MMO to Cyt *c* with ROS production and the importance of the oxidized Cyt *c* in accelerating apoptosis were unveiled. Since Cyt $c_{(ox)}$ is a proapoptotic factor in both the mitochondria-ER and Apaf-1/caspase 9 pathways, modulating the ratio of reduced and oxidized Cyt *c* by introducing appropriate artificial and specific ingredients into the cytosol would be of significance for accelerating apoptosis and killing cells. Additionally, the delivery of Cyt *c*-like molecules to cancer cells might trigger apoptosis independently of Cyt *c* from mitochondria. Thus, the present study may constitute an important step towards developing a rational basis for the design of agents for cancer therapy through pro-apoptotic drugs. Herein, we only focused on the structural alteration of Cyt *c* during its reaction with the MMO or ROS, further study on the structural basis of the MMO including the heme b_5 in Cyt b_5, FAD/FMN in CPR and the heme in CYP might be helpful for a deeper understanding of the mechanism underlying the Cyt *c*-mediated CYP uncoupling.

Authorship

H. X. designed and performed Raman spectroscopic analyses. L. S. and L. C. performed the peroxide assays and ER isolation from mouse liver. S. K. performed component analysis of the RR spectra. J. Z. performed sample preparation in anaerobic conditions. J. T. performed TEM analysis. Y. L. analyzed spectra for H_2O_2 quantification. All authors contributed to prepare the manuscript and approved the final version of the manuscript. P. H. and X. X. H. supervised the whole project.

Funding information

This work was supported by the National Natural Science Foundation of P. R. China (21974054); Project for Science & Technology Development of Jilin Province (20200404189YY). "Talents Cultivation Program" of Jilin University. Further support was provided by the Deutsche Forschungsgemeinschaft (DFG) through the cluster of excellence "Uni-SysCat" under Germany's Excellence Strategy-EXC2008/1–390540038 to P.H. and S.K.

Declaration of competing interest

There are no conflicts to declare.

Appendix A. Supplementary data

Supplementary data to this article can be found online at https://doi.org/10.1016/j.redox.2022.102340.

References

[1] M. Redza-Dutordoir, D.A. Averill-Bates, Activation of apoptosis signalling pathways by reactive oxygen species, Biochim. Biophys. Acta Mol. Cell Res. 1863 (2016) 2977–2992.
[2] D.R. Davydov, Microsomal monooxygenase in apoptosis: another target for cytochrome c signaling? Trends Biochem. Sci. 26 (2001) 155–160.
[3] D.R. Davydov, Microsomal monooxygenase as a multienzyme system: the role of P450-P450 interactions, Expet Opin. Drug Metabol. Toxicol. 7 (2011) 543–558.
[4] R.C. Zangar, D.R. Davydov, S. Verma, Mechanisms that regulate production of reactive oxygen species by cytochrome P450, Toxicol. Appl. Pharmacol. 199 (2004) 316–331.
[5] S.-C. Im, L. Waskell, The interaction of microsomal cytochrome P450 2B4 with its redox partners, cytochrome P450 reductase and cytochrome b(5), Arch. Biochem. Biophys. 507 (2011) 144–153.
[6] H. Zhang, S.-C. Im, L. Waskell, Cytochrome b5 increases the rate of product formation by cytochrome P450 2B4 and competes with cytochrome P450 reductase for a binding site on cytochrome P450 2B4*, J. Biol. Chem. 282 (2007) 29766–29776.
[7] L.D. Gruenke, K. Konopka, M. Cadieu, L. Waskell, The stoichiometry of the cytochrome P-450-catalyzed metabolism of methoxyflurane and benzphetamine in the presence and absence of cytochrome b5(*), J. Biol. Chem. 270 (1995) 24707–24718.
[8] K.K. Rodgers, T.C. Pochapsky, S.G. Sligar, Probing the mechanisms of macromolecular recognition: the cytochrome b5-cytochrome c complex, Science 240 (1988) 1657.
[9] R. Huang, M. Zhang, F. Rwere, L. Waskell, A. Ramamoorthy, Kinetic and structural characterization of the interaction between the FMN binding domain of cytochrome P450 reductase and cytochrome c, J. Biol. Chem. 290 (2015) 4843–4855.
[10] T.M. Hedison, S. Hay, N.S. Scrutton, Real-time analysis of conformational control in electron transfer reactions of human cytochrome P450 reductase with cytochrome c, FEBS J. 282 (2015) 4357–4375.
[11] I.G. Denisov, T.M. Makris, S.G. Sligar, I. Schlichting, Structure and chemistry of cytochrome P450, Chem. Rev. 105 (2005) 2253–2277.
[12] F. Siebert, P. Hildebrandt, Vibrational Spectroscopy in Life Science, Wiley-VCH Weinheim, 2007.
[13] D.H. Murgida, P. Hildebrandt, Disentangling interfacial redox processes of proteins by SERR spectroscopy, Chem. Soc. Rev. 37 (2008) 937–945.
[14] D. Buhrke, P. Hildebrandt, Probing structure and reaction dynamics of proteins using time-resolved resonance Raman spectroscopy, Chem. Rev. 120 (2020) 3577–3630.
[15] T.G. Spiro, Biological applications of Raman spectroscopy, in: Resonance Raman Spectra of Heme Proteins and Other Metalloproteins, vol. 3, John Wiley and Sons Inc., New York, NY, United States, 1988.
[16] T.G. Spiro, in: A.B.P. Lever, H.B. Gray (Eds.), Iron Porphyrins, Part 2, Addison-Wesley, London, 1983, pp. 89–159.
[17] T. Kitagawa, Y. Ozaki, in: J.W. Buchler (Ed.), Structure and Bonding, vol. 64, Springer Berlin Heidelberg, Berlin, Heidelberg, 1987, pp. 71–114.
[18] J. Zhu, M. Jiang, H. Ma, H. Zhang, W. Cheng, J. Li, L. Cai, X.X. Han, B. Zhao, Redox-state-mediated regulation of cytochromec release in apoptosis revealed by surface-enhanced Raman scattering on nickel substrates angew .chem, Int. Educ. 58 (2019) 16499–16503.
[19] X.X. Han, C. Köhler, J. Kozuch, U. Kuhlmann, L. Paasche, A. Sivanesan, I. M. Weidinger, P. Hildebrandt, Potential-dependent surface-enhanced resonance Raman spectroscopy at nanostructured TiO2: a case study on cytochrome b5, Small 9 (2013) 4175–4181.
[20] X.X. Han, A.M. Schmidt, G. Marten, A. Fischer, I.M. Weidinger, P. Hildebrandt, Magnetic silver hybrid nanoparticles for surface-enhanced resonance Raman spectroscopic detection and decontamination of small toxic molecules, ACS Nano 7 (2013) 3212–3220.
[21] Z. Chen, J. Liu, L. Tian, Q. Zhang, Y. Guan, L. Chen, G. Liu, H.-q. Yu, Y. Tian, Q. Huang, Raman micro-spectroscopy monitoring of cytochrome c redox state in Candida utilis during cell death under low-temperature plasma-induced oxidative stress, Analyst 145 (2020) 3922–3930.
[22] N.A. Brazhe, A.B. Evlyukhin, E.A. Goodilin, A.A. Semenova, S.M. Novikov, S. I. Bozhevolnyi, B.N. Chichkov, A.S. Sarycheva, A.A. Baizhumanov, E. I. Nikelshparg, L.I. Deev, E.G. Maksimov, G.V. Maksimov, O. Sosnovtseva, Probing

cytochrome c in living mitochondria with surface-enhanced Raman spectroscopy, Sci. Rep. 5 (2015), 13793.
[23] J. Zhang, W. Xiang, Y. Liu, M. Hu, K. Zhao, Synthesis of high-aspect-ratio nickel nanowires by dropping method, Nanoscale Res. Lett. 11 (2016) 118.
[24] I.G. Denisov, T.M. Makris, S.G. Sligar, I. Schlichting, Structure and chemistry of cytochrome P450, Chem. Rev. 105 (2005) 2253–2278.
[25] D.O. Montellano, R. Paul, Cytochrome P450: Structure, Mechanism, and Biochemistry, Kluwer Academic/Plenum Publishers, New York, 2005.
[26] J.J. Wendoloski, B. Matthew James, P.C. Weber, F.R. Salemme, Molecular dynamics of a cytochrome c-cytochrome b5 electron transfer complex, Science 238 (1987) 794–797.
[27] J. Li, W. Cheng, X. Wang, H. Zhang, J. Jin, W. Ji, X.X. Han, B. Zhao, Electron transfer of cytochrome c on surface-enhanced Raman scattering–active substrates: material dependence and biocompatibility, Chem. Eur J. 23 (2017) 9034–9038.
[28] S. Hu, I.K. Morris, J.P. Singh, K.M. Smith, T.G. Spiro, Complete assignment of cytochrome c resonance Raman spectra via enzymic reconstitution with isotopically labeled hemes, J. Am. Chem. Soc. 115 (1993) 12446–12458.
[29] A. Lawrence, C.M. Jones, P. Wardman, M.J. Burkitt, Evidence for the role of a peroxidase compound I-type intermediate in the oxidation of glutathione, NADH, ascorbate, and dichlorofluorescin by cytochrome c/H2O2: implications for oxidative stress during apoptosis, J. Biol. Chem. 278 (2003) 29410–29419.
[30] P.L. Vandewalle, N.O. Petersen, Oxidation of reduced cytochrome c by hydrogen peroxide, FEBS Lett. 210 (1987) 195–198.
[31] Y. Tan, C.J. Patten, T. Smith, C.S. Yang, Competitive interactions between cytochromes P450 2A6 and 2E1 for NADPH-cytochrome P450 oxidoreductase in the microsomal membranes produced by a baculovirus expression system, Arch. Biochem. Biophys. 342 (1997) 82–91.
[32] I.F. Sevrioukova, T.L. Poulos, Structure and mechanism of the complex between cytochrome P4503A4 and ritonavir, P. Natl. Acad. Sci. USA 107 (2010), 18422.
[33] S. Döpner, P. Hildebrandt, F.I. Rosell, A.G. Mauk, Alkaline conformational transitions of ferricytochrome c studied by resonance Raman spectroscopy, J. Am. Chem. Soc. 120 (1998) 11246–11255.
[34] S. Oviedo-Rouco, M.A. Castro, D. Alvarez-Paggi, C. Spedalieri, V. Tortora, F. Tomasina, R. Radi, D.H. Murgida, The alkaline transition of cytochrome c revisited: effects of electrostatic interactions and tyrosine nitration on the reaction dynamics, Arch. Biochem. Biophys. 665 (2019) 96–106.
[35] V. Yin, G.S. Shaw, L. Konermann, Cytochrome c as a peroxidase: activation of the precatalytic native state by H2O2-induced covalent modifications, J. Am. Chem. Soc. 139 (2017) 15701–15709.
[36] N. Parthasarathi, C. Hansen, S. Yamaguchi, T.G. Spiro, Metalloporphyrin core size resonance Raman marker bands revisited: implications for the interpretation of hemoglobin photoproduct Raman frequencies, J. Am. Chem. Soc. 109 (1987) 3865–3871.
[37] S. Döpner, P. Hildebrandt, A. Grant Mauk, H. Lenk, W. Stempfle, Analysis of vibrational spectra of multicomponent systems. Application to pH-dependent resonance Raman spectra of ferricytochrome c, Spectrochim. Acta A Biomol. Spectrosc. 52 (1996) 573–584.
[38] S. Oellerich, H. Wackerbarth, P. Hildebrandt, Spectroscopic characterization of nonnative conformational states of cytochrome c, J. Phys. Chem. B 106 (2002) 6566–6580.
[39] H.K. Ly, T. Utesch, I. Díaz-Moreno, J.M. García-Heredia, M.Á. De La Rosa, P. Hildebrandt, Perturbation of the redox site structure of cytochrome c variants upon tyrosine nitration, J. Phys. Chem. B 116 (2012) 5694–5702.
[40] S.-R. Yeh, S. Han, D.L. Rousseau, Cytochrome c folding and unfolding: a biphasic mechanism, Acc. Chem. Res. 31 (1998) 727–736.
[41] L. Milazzo, L. Tognaccini, B.D. Howes, G. Smulevich, Probing the non-native states of Cytochrome c with resonance Raman spectroscopy: a tool for investigating the structure–function relationship, J. Raman Spectrosc. 49 (2018) 1041–1055.
[42] W. Lan, Z. Wang, Z. Yang, T. Ying, X. Zhang, X. Tan, M. Liu, C. Cao, Z.-X. Huang, Structural basis for cytochrome c Y67H mutant to function as a peroxidase, PLoS One 9 (2014), e107305.
[43] L.V. Basova, I.V. Kurnikov, L. Wang, V.B. Ritov, N.A. Belikova, I.I. Vlasova, A. A. Pacheco, D.E. Winnica, J. Peterson, H. Bayir, D.H. Waldeck, V.E. Kagan, Cardiolipin switch in mitochondria: shutting off the reduction of cytochrome c and turning on the peroxidase activity, Biochemistry 46 (2007) 3423–3434.
[44] D.F.V. Lewis, P. Hlavica, Interactions between redox partners in various cytochrome P450 systems: functional and structural aspects, Biochim. Biophys. Acta Bioenerg. 1460 (2000) 353–374.
[45] P. Durairaj, J.-S. Hur, H. Yun, Versatile biocatalysis of fungal cytochrome P450 monooxygenases, Microb. Cell Factories 15 (2016) 125.
[46] G. Battistuzzi, M. Borsari, J.A. Cowan, A. Ranieri, M. Sola, Control of cytochrome c redox potential: axial ligation and protein environment effects, J. Am. Chem. Soc. 124 (2002) 5315–5324.
[47] E. Kownatzki, S. Uhrich, P. Bethke, Assessment of ferrocytochrome C oxidation by hydrogen peroxide, Agents Actions 34 (1991) 393–396.
[48] L.M. Brignac-Huber, J.W. Park, J.R. Reed, W.L. Backes, Cytochrome P450 organization and function are modulated by endoplasmic reticulum phospholipid heterogeneity, Drug Metab. Dispos. 44 (2016) 1859–1866.
[49] G.C. Brown, V. Borutaite, Regulation of apoptosis by the redox state of cytochrome c, Biochim. Biophys. Acta Bioenerg. 1777 (2008) 877–881.
[50] Suto Daisuke, Kazuaki, Yoshihiro Sato, Tetsuhiko Ohba, Yoshimura, Junichi, Fujii, Suppression of the pro-apoptotic function of cytochromecby singlet oxygen via a haem redox state-independent mechanism, Biochem. J. 392 (2005) 399–406.

Abbreviation

Apaf-1: apoptotic protease activating factor-1
CPR: cytochrome P450 Reductase
CYP: cytochrome P450
Cyt b_5: cytochrome b_5
Cyt c: Cytochrome *c*
Cyt $c_{(ox)}$: oxidized cytochrome *c*
Cyt $c_{(red)}$: reduced cytochrome *c*
ER: endoplasmic reticula
ET: electron transfer
FAD: flavin adenine dinucleotide
FAM: riboflavin 5′-monophosphate
MMO: microsomal monooxygenase
NADPH: β-Nicotinamide adenine dinucleotide 2-phosphate
ROS: reactive oxygen species
RR: resonance Raman